J Mater Sci (2006) 41:7324–7332
DOI 10.1007/s10853-006-0962-2

Nucleation and growth of small fatigue cracks in filled natural rubber under multiaxial loading

W. V. Mars · A. Fatemi

Received: 20 May 2005 / Accepted: 9 December 2005 / Published online: 17 October 2006

Abstract This paper presents and discusses observations of crack nucleation and small crack growth in a filled natural rubber compound subjected to multiaxial loading. A hollow cylindrical specimen was used in which simultaneous axial and shear strains are produced. The loading path types investigated include axial, torsion, proportional axial-torsion, and non-proportional axial-torsion loadings. It is shown that cracks appear and grow in a particular orientation during a typical fatigue test. The nature and evolution of these cracks with applied cycles were studied by direct observation. The observed failure plane behavior is compared to predictions based on the calculated cracking energy density. Effects of crack closure, load phase angle, crack density, and crack face shearing (mode II), as well as aspects that distinguish between ''nucleation'' and ''growth'' processes in rubber are discussed.

Introduction

The fatigue failure process involves a period during which cracks nucleate in regions that were initially free of observed cracks, followed by a period during which nucleated cracks grow to the point of failure. Analysis approaches that are currently available for predicting fatigue life in rubber, including both crack nucleation as well as crack growth approaches, are reviewed in [1]. The crack growth approach has been studied and used extensively. A practical challenge in applying the crack growth approach to rubber is computation of the energy release rate associated with the crack of interest, and predicting the location and path of the fastest growing crack, especially when the geometry and loading are complicated.

This paper presents and discusses observations of crack nucleation and small crack growth in a natural rubber compound filled with carbon black subjected to multiaxial loading. Small cracks are often of particular importance, since most of a component's life is typically consumed while cracks are small relative to other component features. A hollow cylindrical specimen was used in which simultaneous axial and shear strains are produced via independently controlled axial and twist displacements. The multiaxial loading path types investigated include axial loading, torsion loading, proportional axial-torsion loading, and non-proportional axial-torsion loading. These loading paths are shown in Fig. 1. Details of the experimental procedure and loading conditions used are discussed in [2, 3].

This paper presents evidence supporting the view that fatigue crack nucleation in rubber results from the growth of flaws already present in the virgin material. It is also shown that cracks appear and grow in a particular orientation, during a typical fatigue test of the type investigated. The nature and evolution of these cracks with applied cycles were studied by direct observation. It is demonstrated that cracking energy density (CED) can rationalize the observed failure

W. V. Mars
Cooper Tire and Rubber Company, 701 Lima Avenue, Findlay, OH 45840, USA

A. Fatemi (✉)
MIME Department, MS 312, The University of Toledo, 2801 W Bancroft Street, Toledo, OH 43606, USA
e-mail: afatemi@eng.utoledo.edu

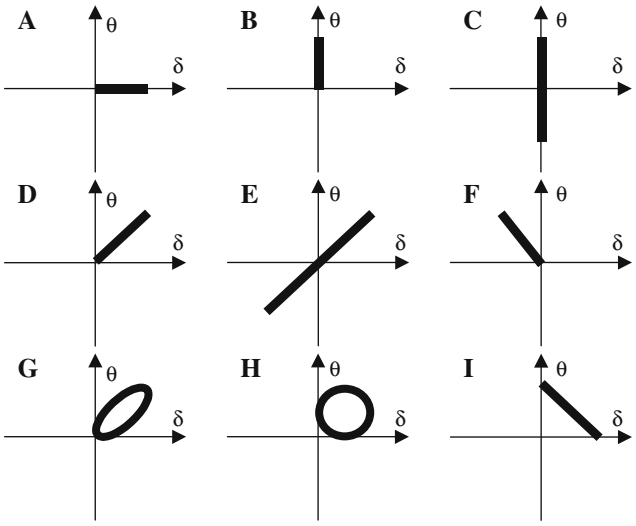

Fig. 1 Axial-torsion load paths and designations used. δ is axial displacement, θ is twist angle, and P is axial load

plane behavior. Aspects that distinguish between ''nucleation'' and ''growth'' processes in rubber are also discussed. The ability of various estimates of the crack driving force to correlate results from fatigue growth rates of nucleated cracks from different multiaxial loading paths is considered in another publication [4].

Pre-existing flaws as crack nucleation sites

It has long been understood that the fatigue failure of elastomers is due to the growth of flaws existing in the initial material [5]. In rubber, this view is supported by the general agreement between several independent techniques for observing and/or estimating the size of such flaws [5–8]. These include direct observation via techniques such as optical microscopy and SEM, and indirect techniques involving the extrapolation of fatigue or strength measurements on specimens with controlled flaw sizes to specimens without intentional flaws. In practice, the precise nature of such flaws remains obscure because there are multiple sources of flaws in the observed size range. These sources include filler agglomerates [8], compound additives, mold release agents, impurities occurring naturally in the raw elastomer [7], and imperfections in mold surfaces [5].

In this study, Scanning Electron Microscopy (SEM) was conducted on the surfaces of the virgin material in an unloaded specimen, as well as on a specimen, which had been failed in fatigue. Inspection of the virgin surface in Fig. 2a shows that surface cavities in the expected size range (of order 0.1 mm) are observed. Slightly smaller non-rubber particles or inclusions are

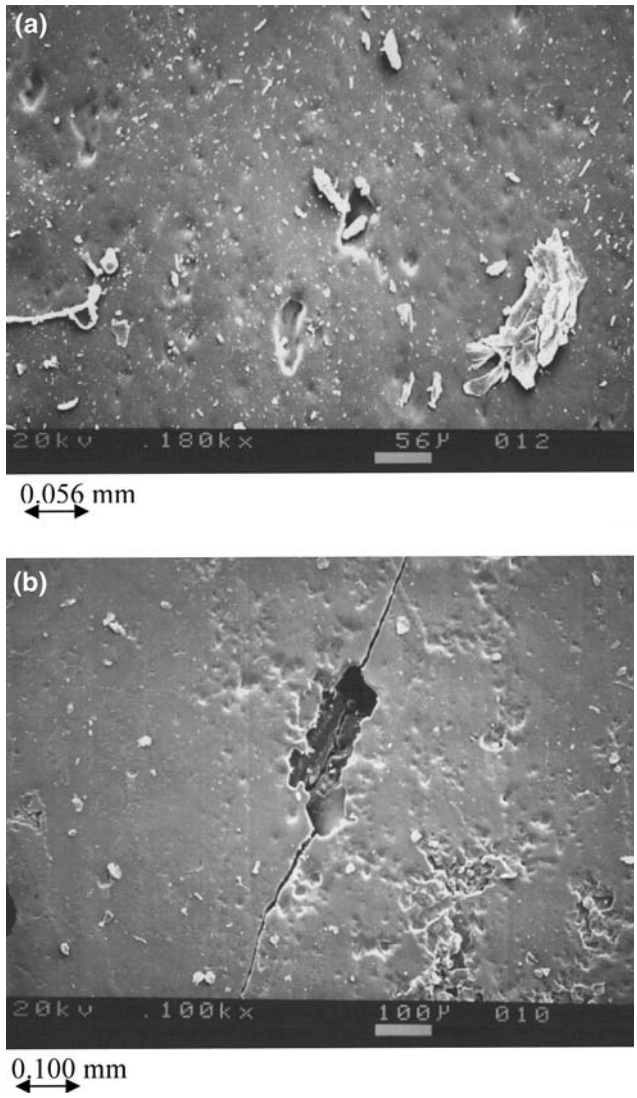

Fig. 2 (**a**) Naturally occurring voids and inclusions on a virgin specimen surface at 180×. (**b**) Crack emanating from a naturally occurring void on a failed specimen surface at 100×

also observed at the surface of the specimen. Some of these apparently penetrate the specimen surface. It is believed that these particles may be mold release agents used during the curing process.

Inspection of the failed specimen in Fig. 2b gives direct evidence that nucleation proceeds from pre-existing crack nucleation sites. A sharp crack is shown emanating from a void. The crack extends along the surface, and into the depth of the specimen (as can be seen in the bottom of the void), suggesting a half-penny-shaped crack geometry. There can be little doubt that such sites are the precursors to visible cracks that lead to failure.

The volumetric and area density of flaws depends on the flaw size of interest. For the voids and inclusions shown in Fig. 2, the flaw density per unit area is very

roughly estimated to be in the range 2 defects/mm^2 (for flaws of $\approx$ 0.1 mm) to 300 defects/mm^2 (for flaws of $\approx$ 0.02 mm). If the volumetric flaw density is assumed to be given roughly by the –3/2 power of area flaw density, as it would for flaws distributed on a cubic lattice, then the volumetric densities lie in the range $(2)^{-3/2} \approx 3$ defects/mm^3 (for flaws of $\approx$ 0.1 mm) to $(300)^{-3/2} \approx 5{,}000$ defects/mm^3 (for flaws of $\approx$ 0.02 mm). Presumably, this approach would overestimate volumetric flaw density, because free surfaces have opportunities to collect additional flaws during manufacture and use.

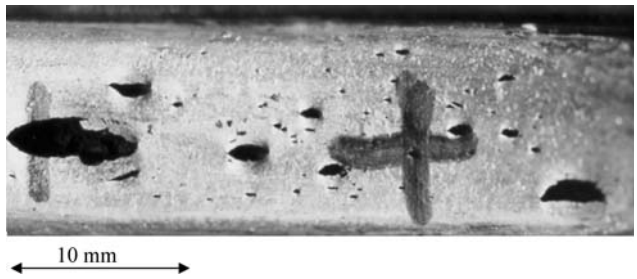

Fig. 3 Typical failure planes for pure $R = 0$ axial loading (path A)

Crack nucleation

One general observation that can be made regarding the formation of cracks on the axial-torsion specimen surfaces, independent of multiaxial strain history type, is that the cracks form on a specific plane, or in certain cases, on several specific planes. For proportional $R = 0$ histories (such as path D in Fig. 1), the observed cracking plane was oriented perpendicular to the direction of maximum tensile strain. For more complex histories, preferred nucleation planes were still observed, but their relationship to the principal strain directions was sometimes different.

Traditional approaches for multiaxial fatigue crack nucleation analysis in rubber such as the strain energy density are based on criteria that make no reference to a specific material failure plane. Therefore, an analysis approach that makes specific reference to the failure plane, such as the CED criterion is better suited in crack nucleation life analyses of multiaxial strain histories [3, 9]. CED represents the portion of the strain energy density that is available to be released by virtue of crack growth on a specified material plane (i.e. failure plane). The calculation of CED, and the rationale for interpreting it as available energy density, is discussed in [10].

Since the CED accounts for the stresses and strains experienced by a specific material plane, it provides a way to predict the failure plane. For proportional histories, the material plane that maximizes the CED is perpendicular to the direction of maximum principal strain. The CED may also be applied in cases where the history is non-proportional. In this section, the observed failure plane behavior is presented and it is demonstrated that the CED can rationalize the observed failure plane behavior.

Axial and torsion loadings

In axial tests, crack initiation was consistently observed on a single plane, transverse to the direction of maximum principal strain, see Fig. 3. This plane also maximizes the CED. In $R = 0$ torsion tests (path B), crack initiation also exhibited a well-defined failure plane, with a typical example shown in Fig. 4. The orientation, in the undeformed state, of the failure

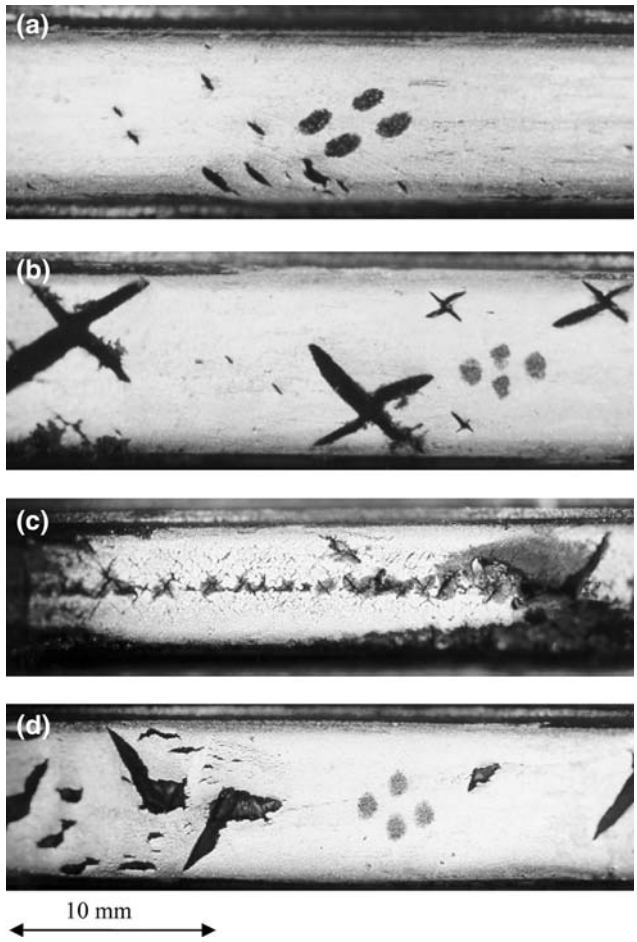

Fig. 4 Typical failure planes for torsion loading. (**a**) Cyclic torsion with $R = 0$ (path B). (**b**) Cyclic torsion with $R = -1$ (path C). (**c**) Cyclic torsion with $R = -1$ and a static axial compression load (path J). (**d**) Cyclic torsion with $R = -1$ and a static axial tension load (path K)

plane ranged from $\alpha = 34°$ for the longest life tests to $\alpha = 19°$ in the shortest life tests. Cracks images were made in the deformed state, typically at the mean deformed state. Herein, orientation is quantified as the angle between the crack and the horizontal axis, and defined as positive in the clockwise direction.

A plot of the variation of CED with cracking plane orientation based on theoretical calculations is shown in Fig. 5, for several levels of twist in torsion tests. It can be seen that, for $R = 0$ torsion histories, a single plane of maximum CED is predicted that may theoretically range between $\alpha = 0°$ and $\alpha = 45°$. For finite strains, a state of pure shear strain cannot be achieved because the axial strain component depends on the sum of the squares of the shear components (from the definition of the Green LaGrange strain). Thus, the principal strain directions associated with finite strain torsion rotate as the ratio of the shear strain component changes with respect to the axial component. For infinitesimal strains, the CED criterion predicts cracking on the 45° plane, as observed in torsion fatigue of high strength, low ductility metals. For very large shear strains, the failure plane approaches $\alpha = 0°$, since the axial strain component dominates the response at very large shear strains. The significant rotation of the failure plane, even at relatively long life demonstrates the critical need to account for finite strains in rubber fatigue. Careful accounting must be made of the fact that the cracking plane is embedded in the material, and may rotate during straining.

Comparison of $R_\theta = 0$ torsion tests (path B) with $R_\theta = -1$ torsion tests (path C) provides valuable insight on the mechanics of the fatigue process. Figure 6 shows that while the $R_\theta = 0$ curve exhibits a single maximum of the CED at $\alpha \approx 36°$, the $R_\theta = -1$ curve exhibits two maxima, at $\alpha \approx 36°$ and at $\alpha \approx 144°$. These maxima correspond to two distinct planes that have the same CED history, and thus are equally favorable to crack initiation. These failure plane predictions agree quite well with experiments, as shown in Fig. 4b for path C, in the form of a ''star crack.''

Figure 4 also shows failed specimen surfaces associated with paths J and K, where fully reversed $R_\theta = -1$ twist-controlled torsion was applied in combination with a load-controlled static compression (path J), or a static tension (path K). These tests were conducted to investigate the effects of crack closure. In the case of static compression (path J), enhanced closure is suggested by visible evidence of crack face rubbing (note wear debris, and ''erasure'' of silver ink from the specimen surface in the vicinity of cracks in Fig. 4c). No evidence of crack face rubbing is observed in the case of static tension (path K). Path K shows evidence of non-self similar crack growth, which is known to be

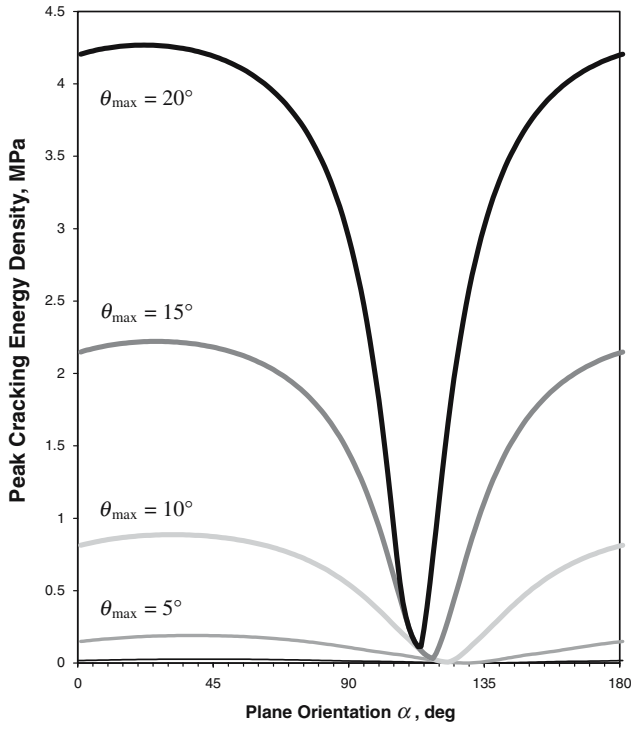

Fig. 5 Effect of plane orientation α on peak CED for several levels of twist displacement θ in cyclic torsion tests with $R = 0$

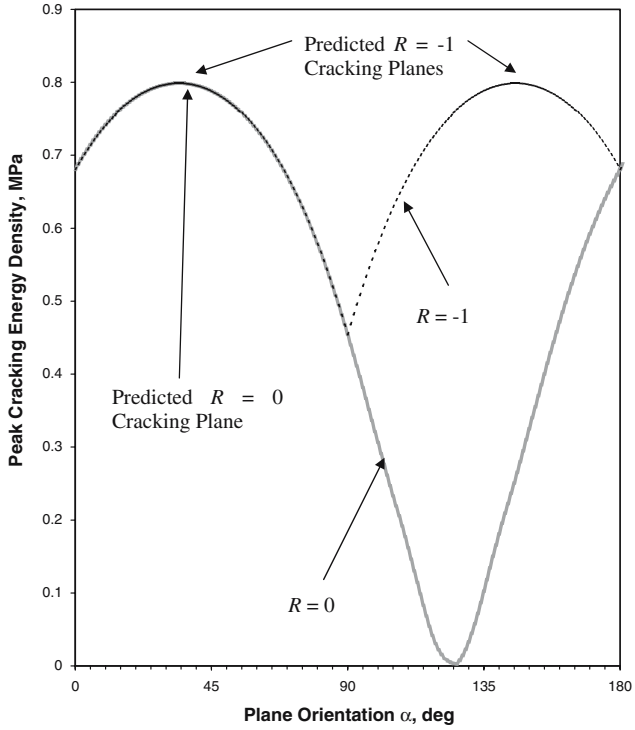

Fig. 6 Effect of plane orientation α on peak CED for $R = 0$ and $R = -1$ cyclic torsion tests

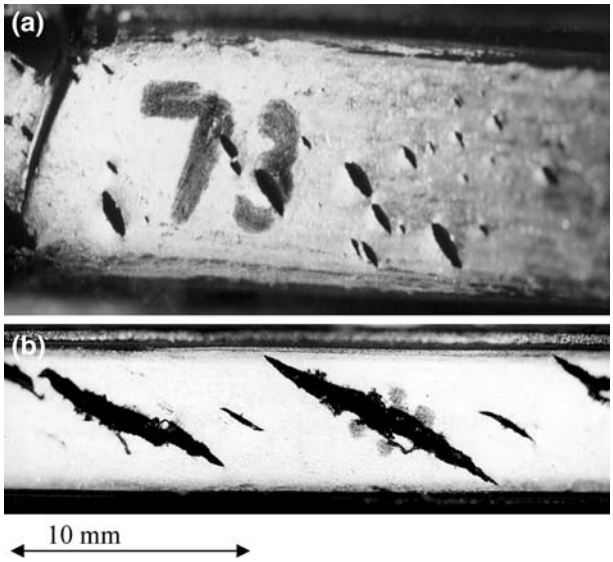

Fig. 7 Typical failure planes for proportional axial-torsion loading with $R = 0$ (paths D) in (**a**) and with $R = -1$ (path E) in (**b**)

associated with crack growth under $R > 0$ loading conditions [11].

A comparison of $R = 0$ and $R = -1$ torsion loading also underscores the importance of accounting for crack closure in fatigue analysis. For example, if no closure criterion is used, the energy density computed on material planes experiencing compression will be positive. In this case, $R = 0$ torsion will also exhibit two planes of maximum energy density, one associated with the plane on which flaws are opening in tension, and another associated with the plane on which work is being done in compression against closed crack faces. The fact that a single cracking plane, associated with the maximum tensile strain direction is observed for $R = 0$ torsion shows that the energy density stored on the compressive plane is not available for the growth of flaws.

Proportional and non-proportional loadings

As already discussed, in the case of finite strain torsion, an axial strain component exists which causes rotation of the failure plane. In proportional axial-torsion strain histories, the additional axial strain may be introduced independently of the shear strain, but has a similar effect on the orientation of the failure plane. As the axial strain component increases relative to the shear strain component, the crack nucleation plane becomes closer to $\alpha = 0°$. This trend was clearly observed in $R = 0$ axial-torsion experiments run at two proportional ratios of shear engineering strain to axial engineering strain, 0.25 and 0.50, as shown in Fig. 7a for path D. Note that a single crack initiation plane is observed, which is in agreement with the CED predictions.

Several $R = -1$ proportional axial-torsion experiments were also run, path E. Due to the crack closure effect in the compression segment of the displacement cycle, and because of stiffening of the stress-strain response in compression, the previously discussed symmetry of the CED history for the case of fully reversed torsion does not apply here. A single cracking plane is therefore predicted, and was observed in path E tests. Typical crack nucleation planes for tests using path E are shown in Fig. 7b. In the path E tests, the presence of crack face friction associated with the torsion-compression portion of the loading cycle was evidenced by wear debris.

Non-proportional histories were investigated in which $R = 0$ axial and torsion displacements were applied at varying phase angle ϕ. Figure 8 shows results for paths G ($\phi = 45°$), H ($\phi = 90°$), and I ($\phi = 180°$). It was generally found that the phase angle had little effect on the failure plane, at least for $\phi \leq 90°$. Based on the maximum CED criterion, the predicted cracking plane also shows little dependence on ϕ, as shown in Fig. 9.

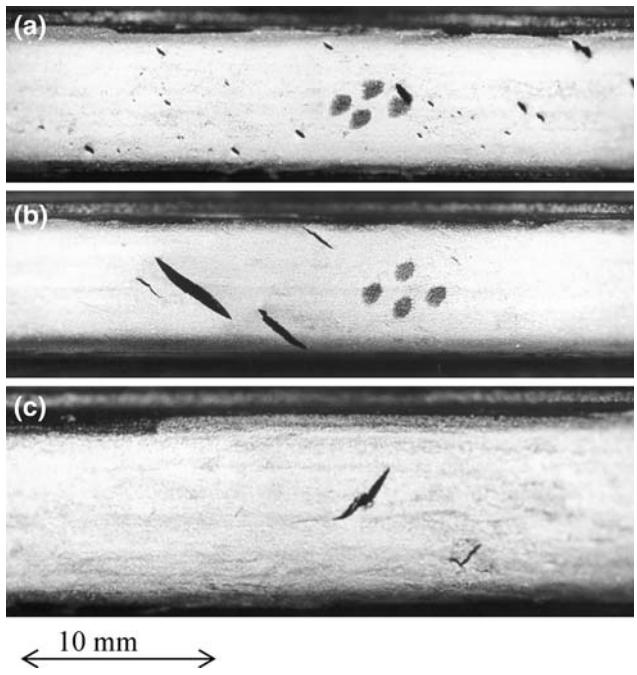

Fig. 8 Typical failure planes for out-of-phase axial-torsion loading with $R = 0$ for both axial and torsion loads. (**a**) 45° out-of-phase (path G), (**b**) 90° out-of-phase (path H), and (**c**) 180° out-of-phase (path I)

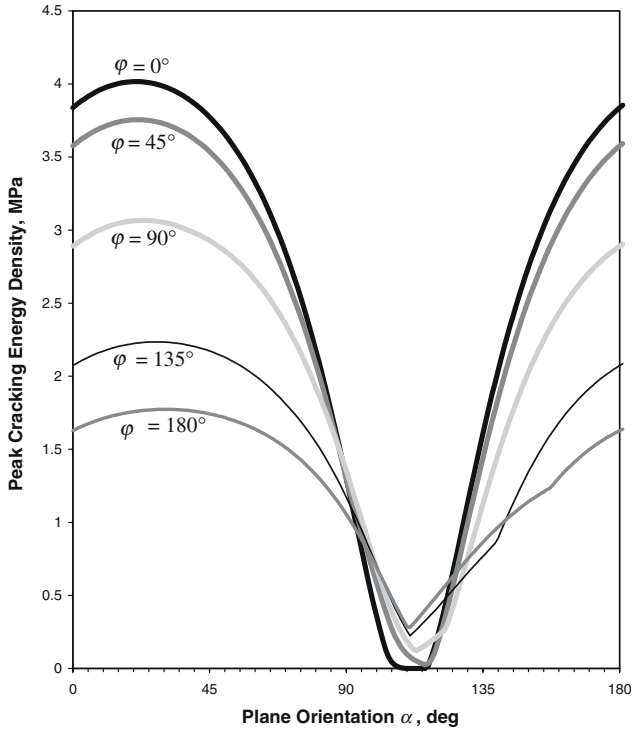

Fig. 9 Effect of phase angle ϕ on the relationship between peak CED and plane orientation α

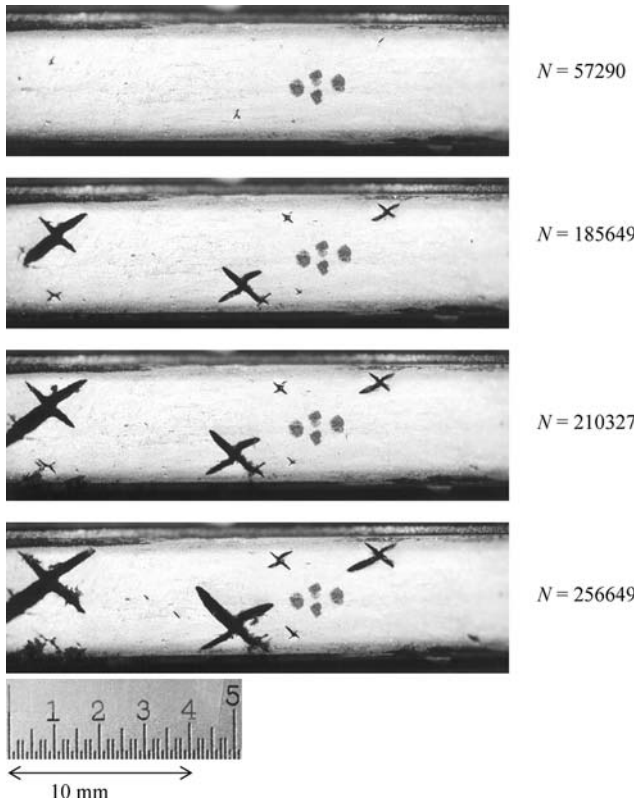

Fig. 10 Crack nucleation and growth in a torsion test with R = –1 (path C)

For the $\phi = 180°$ out-of-phase condition (path I), crack initiation plane occurred at $\alpha = -50° = 130°$, as shown in Fig. 8c. The predicted plane at 32° does not coincide with the observed failure plane. More accurate models for the non-linear elastic behavior, rather than the Neo-Hookean model used in this study, and accounting for the inelastic effects associated with rubber constitutive behavior may improve the predictive capability of the CED criterion.

Crack growth

In a typical test, multiple cracks developed, approximately in a uniform manner around the circumference of the specimen. The evolution of surface cracking with applied cycles was recorded photographically. The number of measured cracks obtained per photograph ranged from 1 to 8. The photographs capture approximately 10% of the specimen circumference.

Typical examples of crack initiation and growth for loading paths C and H are shown in Figs. 10 and 11, respectively. Corresponding crack length versus cycle histories for these paths are shown in Figs. 12a and b, respectively.

The photographic images give a rough sense of the crack density at failure, which reflects the combined influences of the initial flaw density, and the subsequent evolution of the flaw density through processes such as crack coalescence and shielding. Coalescence is a process whereby individual cracks join to form a larger, single crack. Shielding is a process whereby the growth of smaller cracks is arrested by larger adjacent cracks. These processes are shown schematically in Fig. 13. Instances of both processes can be seen in the photographic sequences given in Figs. 10 and 11.

Surface crack densities near specimen failure were estimated from the last photograph taken from each test. These were computed from the number of visible cracks and specimen surface area visible in each photograph ($\approx$200 mm^2). Visible cracks were only counted if their length was at least 0.5 mm. The largest cracks at specimen failure were not usually larger than 10 mm. The resulting crack densities ranged from 0.005 to 2.4 cracks/mm^2. These values are generally much smaller than the flaw densities estimated in Section ''Pre-existing flaws as crack nucleation sites,'' which suggests that a significant fraction of the flaws counted in Section ''Pre-existing flaws as crack nucleation sites'' experienced little or no growth.

As noted in Section ''Crack nucleation,'' crack nucleation occurs on a specific plane (or on several

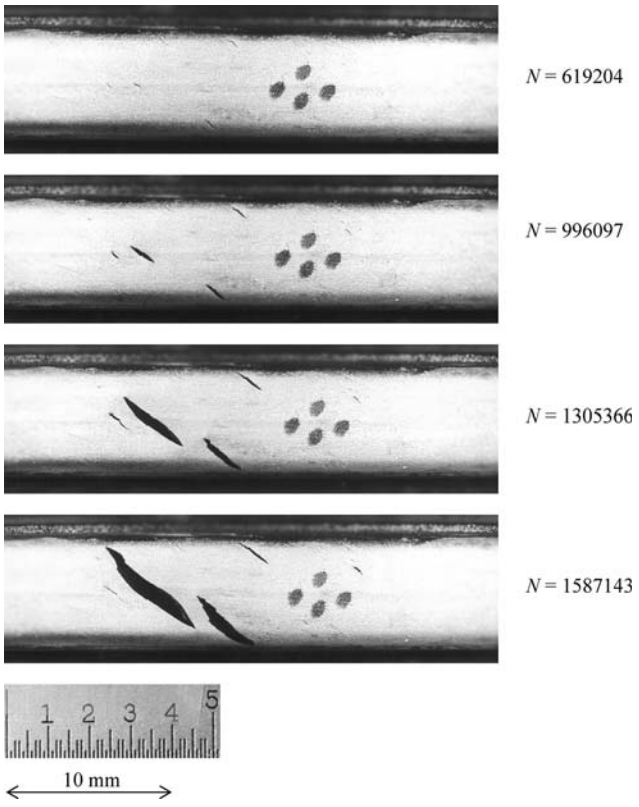

Fig. 11 Crack nucleation and growth in a 90° out-of-phase axial-torsion test with $R = 0$ (path H)

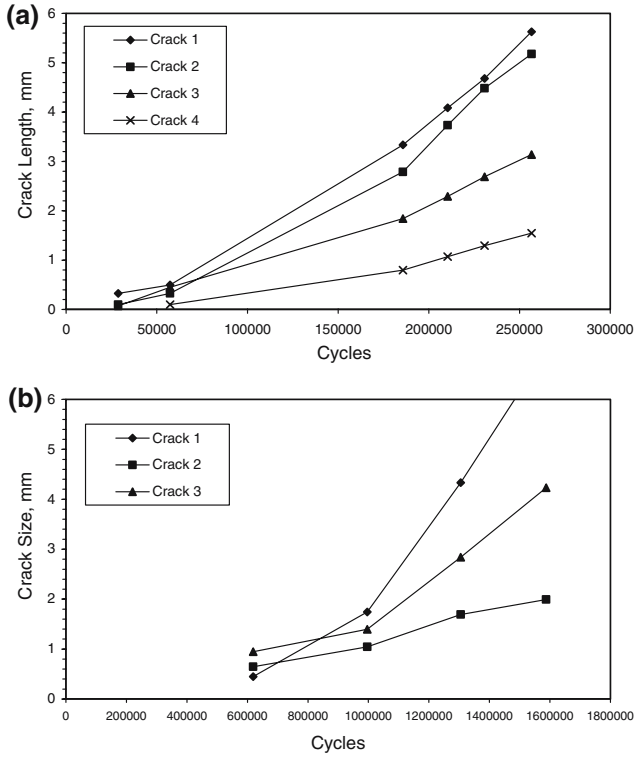

Fig. 12 Crack growth histories in (**a**) torsion test with $R = -1$ (path C), and in (**b**) 90° out-of-phase axial-torsion test with $R = 0$ (path H)

specific planes). In most cases, crack growth exhibited substantial self-similarity, from the earliest stages of observed initiation, to the final stages when the crack growth rate was strongly influenced by specimen boundaries.

Note that for paths B, C, D, E, and H, certain amounts of crack face shearing (mode II) were present in the load history, on the cracking plane. While the presence of mode II loading often implies crack path deviation, this was not observed in the present results. This may be attributed to the following considerations. First, on the cracking plane, mode I loading was dominant. Second, cracking planes on which non-self-similar growth would be favored tend to become reoriented by virtue of the non-self-similar growth in such a way that self-similar growth is again favored. Cracks on such planes also would grow more slowly than cracks on planes favorable to self-similar growth. If such crack deviation and/or reorientation occurs, it must be very early in life, as no instances were observed in this study.

All experimentally observed crack growth histories exhibit substantially similar evolution with applied cycles, as shown in Fig. 12. Characteristically, very few cracks were visible in the photographs during the first 1/3 of the life. The smallest measurable features in the photographs were approximately 0.026 mm in length. At specimen failure, cracks typically reached a length in the range of 1–10 mm. From Figs. 10 and 11 it can be seen that a relatively large range of crack sizes is developed at failure. It is hypothesized that the range primarily reflects variation of the initial effective lengths of the cracks. Since the energy release rate varies with the size of the crack, the range of observed crack sizes increases with life fraction.

Crack nucleation versus crack growth

In fatigue analysis, it is traditional to distinguish two phases of damage development: the crack nucleation phase (in which cracks appear), and the crack growth phase (in which cracks grow). The evidence examined in this work was consistent with the claim that the appearance of visible cracks in rubber is caused by the growth of initially unobserved flaws. Assuming this is true, it seems natural to consider whether the term ''nucleation'' is an appropriate description of the process. The term ''nucleation'' implies a precursor process, sometimes also called

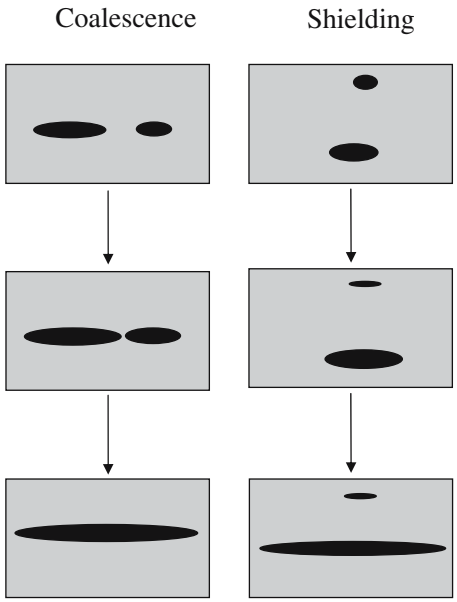

Fig. 13 Schematics of crack coalescence and shielding processes

''early growth,'' that is somehow distinct from the subsequent crack growth process. In contrast, it appears that the crack growth process in rubber is governed at all times by a characteristic fatigue crack growth curve.

Two aspects may be said to distinguish ''nucleation'' and ''growth'' processes in rubber. First, the flaws from which crack growth initiates do not usually possess a well-defined crack tip, while subsequent growth does. In analysis, however, this fact can often be accommodated without reference to distinct nucleation and growth phases, by selecting an effective initial flaw size that reflects both the average size and bluntness of initial flaws.

A second aspect that may be said to distinguish nucleation and growth processes for rubber is the dependence of the energy release rate on the size of the crack. During nucleation, the driving force for flaw growth varies in direct proportion to the size of the flaw, and to the magnitude of the far-field loading, independent of any far-field boundaries or stress/strain gradients. Flaw growth during nucleation is very sensitive to factors such as the geometry of initial flaws, the microstructure of the material, and the applicability of the continuum assumption, which explains the variability inherent in observations of crack nucleation. After nucleation, the crack driving force becomes dependent on geometrical factors associated with specimen boundaries and with stress/strain gradients. Thus, the variation of the crack driving force with crack size after nucleation can only be determined via considerations specific to the geometry and loading of the particular crack / component system. This approach to distinguishing nucleation and growth is somewhat dependent on the size of the specimen or component.

Using the latter definitions of nucleation and growth, it may be said that crack nucleation and small crack growth (<1 mm for the present specimen) often occupy a significant portion of the fatigue life. This is because the initial flaws are typically much smaller than component features, and are small relative to stress/strain field gradients. Also, the transition to the long crack (>3 mm for the present specimen) growth phase often implies the presence of cracks large enough to cause part failure. For the axial-torsion specimen, the crack nucleation phase occupied the first half of life, and the crack growth phase occupied the final half of life.

Conclusions

1. Crack nucleation in rubber proceeds from pre-existing flaws in the virgin material, such as voids or surface cavities and non-rubber particles or inclusions. These flaws act as crack nucleation sites, which are the precursors to visible cracks that lead to failure.
2. Multiple cracks typically developed, approximately in a uniform manner around the circumference of the specimen. Observations of crack density at failure reflect the combined influences of the initial flaw density and the subsequent evolution of the flaw density through processes such as crack coalescence and shielding.
3. Very few cracks were visible during the first 1/3 of the life. The smallest measurable features in the photographs were approximately 0.03 mm in length, while at specimen failure cracks typically reached a length in the range of 1–10 mm. The crack nucleation phase occupied the first half of life, and the crack growth phase occupied the final half of life.
4. Fatigue crack nucleation and growth in rubber occurs on preferred failure plane(s). In most cases, crack growth exhibited substantial self-similarity, from the earliest stages of observed initiation, to the final stages when the crack growth rate was strongly influenced by specimen boundaries.
5. For axial, torsion, and proportional axial-torsion strain histories investigated, the observed cracking plane was oriented transverse to the maximum principal strain direction. For more complex histories, preferred nucleation planes were still observed,

but their relationship to the principal strain directions was sometimes different.

6. CED rationalizes the observed failure plane behavior across a wide range of states, and relates physically to the fracture mechanical behavior of small flaws under complex loading.
7. The effects of finite strain were manifest as a tendency of the failure plane to appear in an orientation closer to the pure axial failure plane, than would be expected from small strain theory. This demonstrates the critical need to account for finite strains in rubber fatigue and realization of the facts that the cracking plane is embedded in the material and can rotate during straining.
8. The presence of crack closure influences the crack nucleation plane. Enhanced closure was observed by visible evidence of crack face rubbing in cyclic torsion with static compression. Crack closure due to crack face friction also occurred in fully reversed axial-torsion tests during the torsion-compression portion of the loading cycle, as evidenced by wear debris.

References

1. Mars WV, Fatemi A (2002) Int J Fatigue 24:949
2. Mars WV, Fatemi A (2004) ASME J Eng Mater Technol 126:19
3. Mars WV, Fatemi A (2005) J Fatigue Fract Eng Mater Struct 28:523
4. Mars WV, Fatemi A Rubber Chem Technol (to appear)
5. Gent AN, Lindley PB, Thomas AG (1964) J Appl Polym Sci 8:455 (Reprinted in Rubber Chem Technol 38, 1965, pp 292–300)
6. Lake GJ, Lindley PB (1965) J Appl Polym Sci 9:1233 (Reprinted in Rubber Chem Technol 39, 1966, pp 348–364)
7. Choi IS, Roland CM (1996) Rubber Chem Technol 69:591
8. Dizon ES, Hicks AE, Chirico VE (1974) Rubber Chem Technol 47:231
9. Mars WV, Fatemi A (2005) J Fatigue Fract Eng Mater Struct 28:515
10. Mars WV (2005) Heuristic approach for approximating energy release rates of small cracks under finite strain multiaxial loading In: Coveney V (Ed.), Elastomers and components—Service life prediction; progress and challenges, OCT Science, Philadelphia, pp 89–109
11. Busfield JJC, Ratsimba CHH, Thomas AG (1999) Crack growth and predicting failure under complex loading in filled elastomers. In: Boast D, Coveny VA (Eds.), Finite element analysis of elastomers, published by IMechE, UK pp 235–250